Tunable Fano resonance and magneto-optical response in magnetoplasmonic structure fabricated by pure ferromagnetic metals

Leyi Chen,[1] Jinlong Gao,[1] Wenbin Xia,[1] Shaoyin Zhang,[1,2] Shaolong Tang,[1,*] Weiyi Zhang,[1] Daoyong Li,[1,2] Xiaoshan Wu,[1] and Youwei Du[1]

[1]*Collaborative Innovation Center of Advanced Microstructures, Jiangsu Key Laboratory for Nanotechnology, Nanjing National Laboratory of Microstructures, and Department of Physics, Nanjing University, Nanjing 210093, People's Republic of China*

[2]*School of Science, Institute of Condensed Matter Physics, Linyi University, Linyi 276005, Shandong, People's Republic of China*

(Received 29 July 2015; revised manuscript received 31 March 2016; published 13 June 2016)

The developments in nanophotonics demand more efficient and delicate control of light. It has recently been proposed to achieve this goal by combining plasmonics and magneto-optics in so-called magnetoplasmonic nanostructures. However, significant challenges still remain because of the difficulty in the design of spectrally tunable systems exhibiting novel plasmonic and magneto-optical responses simultaneously. Here we report a magnetoplasmonic structure which consists of a two-dimensional nickel nanodisk array on top of a cobalt film substrate. We demonstrate that a tunable Fano resonance can be generated in this system with properly designed geometric parameters. Furthermore, the magneto-optical Kerr responses in this system can be manipulated due to the concerted actions of free electrons in the resonance. Our results reveal the possibility of fabricating large-area magnetoplasmonic structures by a simple, mass-producible method, and tuning the plasmonic and magneto-optical responses simultaneously.

DOI: 10.1103/PhysRevB.93.214411

I. INTRODUCTION

In the last decade, we have witnessed the booming development of plasmonics in which light is concentrated and manipulated in the subwavelength scale due to the excitation of surface plasmons (SPs). Particularly, magnetoplasmonic nanostructures have so far drawn great attention due to their multifunctionality that allows active control of SPs and significant enhancement of magneto-optical (MO) effects [1–5]. This leads to a wide range of applications in ultrasensitive molecular detection [6,7], nanoantennas [8], all-optical magnetic data storage [9], optical isolators and modulators [10,11], ultraprecise distance probe [12], etc. Single particles can tailor the amplitude and sign of the MO response via localized surface plasmons (LSPs) that are sensitive to the variations in size and shape [13]. The surface plasmon polaritons (SPPs), on the other hand, are propagating electromagnetic waves bound to the interface between metals and dielectrics. Interestingly, two or more coherent SP modes may coexist in a complex plasmonic system, resulting in a fascinating Fano resonance. Compared with the conventional simple resonance modes, the Fano resonance possesses a steep, asymmetric line shape and an inherently excellent sensitivity to the changes in geometry or dielectric environment [14–16].

So far, the investigations related to magnetoplasmonic nanostructures mainly focused on the demonstration of the excitation of either LSPs [6,17–21] or SPPs [22–29], and consequently the enhancement of MO responses. An inevitable problem that appears in most of these nanostructured systems is the essentially reduced volume fraction of ferromagnetic (FM) materials compared with continuous film or bulk. Even if the MO response is enhanced due to SPs, the incorporation of non-FM materials would nevertheless dilute the influence of SPs and accordingly weaken the overall MO response. A direct strategy to solve this problem is to develop coupled plasmonic systems containing FM metals exclusively, in which the overall MO response may be manipulated by Fano resonance. Therefore, it is of particular interest to implant the Fano resonance into magnetoplasmonic systems, as it has the potential to offer more novel plasmonic and MO properties with outstanding controllability. However, very few works revealed the Fano-type spectra in magnetoplasmonic systems, which are mostly related to the interference between SPP modes [9], the interaction between the LSP modes that originated from different parts [30], or the interaction between the LSP mode and the Rayleigh anomalies [31]. These kinds of Fano resonances cannot be freely tuned unless the geometric parameters of the nanostructures are changed. The primary challenge for convenient tunability in the design of Fano resonance is the spectral engineering via controlled coupling of proper plasmon modes. This difficulty is more severe when taking into account the strong damping of SPs in FM metals arising from the large imaginary part of their dielectric constant.

In this work, we introduce another perspective on magnetoplasmonics by directly constructing a two-dimensional (2D) ordered Ni nanodisk array on top of a Co film. We demonstrate that a properly designed size and periodicity of the nanodisks can lead to the Fano resonance, resulting from the strong coupling between spectrally overlapped LSP and SPP modes. We also show how the Fano resonance can be delicately tuned and further, how the concerted actions of free electrons in the resonance can modify the MO response of the whole system.

II. DESIGN AND FABRICATION

The microscopic origin of Fano resonance arises from the strong interaction between a narrow discrete resonance and a spectrally overlapping broad one or continuum [14]. For a plasmonic structure made of conventional plasmonic

*Corresponding author: tangsl@nju.edu.cn

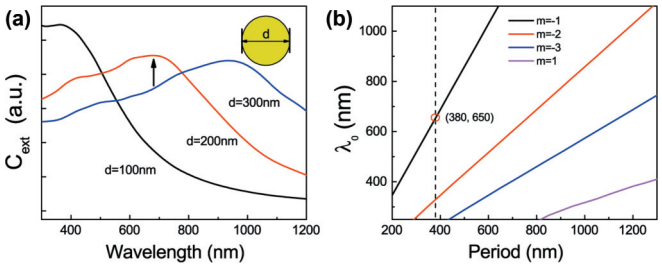

FIG. 1. Spectral properties of LSPs and SPPs. (a) Calculated extinction cross sections C_{ext} versus wavelength for 125-nm-high Ni nanodisks with 100, 200, and 300 nm diameters by the FDTD method. (b) Calculated period dependence of the spectral positions λ_0 to excite SPPs at the air-metal (Co) interface according to the momentum match condition. m is the integer for the diffraction order. The incident angle of light is set to 45°.

materials such as Ag or Au, these conditions can be easily satisfied due to the existence of a variety of LSP modes [32,33]. However, the damping of typical FM metals (such as Fe, Co, and Ni) is too large to provide a relatively sharp LSP resonance. As demonstrated in Fig. 1(a), where the extinction cross sections of Ni nanodisks are calculated by the finite-difference time-domain (FDTD) method, the dipole mode of the LSPs resonance spans over more than 200 nm spectral range and it shows a redshift behavior as the diameter increases. The same results can be obtained via calculating the polarizability of the cylinder [34]. Higher multipolar plasmon modes in noble metals are usually narrower than the dipole mode, but that cannot be clearly observed in FM particles. Moreover, the spectral position of LSPs depends on the size and shape of the particle, which requires additional tedious nanofabrication procedures. Therefore, the LSP mode is not an appropriate way to provide the sharp resonance for realizing tunable Fano resonance. On the contrary, the SPP mode is a proper alternative due to its well-defined spectral positions and convenient tunability by changing the momentum match condition. As we know, the SPPs cannot be generated by the light that directly impinges on a metal surface due to the momentum mismatch. A proper way to provide the missing momentum is to use the reciprocal lattice vector of periodic arrays [35]. Accordingly, the spectral positions to generate SPPs for a given order can be exactly predicted and tuned to overlap with the LSPs. The calculated period dependence of the spectral positions is plotted in Fig. 1(b).

For the reasons given above, we propose a magnetoplasmonic system containing an ordered Ni nanodisk array on the top of a Co film. The nanodisks and the periodic arrangement can provide the broad LSP and sharp SPP modes, respectively, satisfying the conditions for Fano resonance. The geometric parameters of the system are determined according to the calculated results in Figs. 1(a) and 1(b), which are a 200 nm diameter of nanodisks and a 300–400 nm period of the array, optimizing for an effective coupling in the 500–700 nm region. It is worth mentioning that the use of 2D ordered nanodisks has two major advantages over the simple 1D periodic nanowires. One is the relatively weak magnetic shape anisotropy that may lead to a high saturation field, especially perpendicular to the wires. The other is that the spectral positions of LSPs for individual nanodisks are stable when we change the momentum match condition of SPPs, which favors a better control of Fano resonance. In addition, the choice of Ni is based on the recent reports related to the novel MO responses which can be tuned by the phase of LSPs in Ni nanodisks [6,17], as well as the excellent compatibility with the electrochemical deposition process used in our experiments. The Co bottom layer is employed because it sustains relatively stronger MO effects than other FM metals. It has to be mentioned that the height of the nanodisk is a crucial factor for the emergence of effective LSPs, because the Ni nanodisks are directly built on a metal film instead of a dielectric substrate. If the height is not sufficiently high, the collective oscillation of the free electrons on the nanodisks induced by the incident light will rapidly transfer to the Co film, which will hinder the excitation of effective LSPs. Therefore, the height of the nanodisks is set to be 125 nm.

To construct highly ordered nanostructures, interference lithography was adopted in our experiments, which is based on the interference of two laser beams that can produce a fringe pattern used to expose a photoresist layer without any mask [36,37]. Figure 2(a) shows the topography of the photoresist pattern on top of a 50-nm-thick Co film. A square array of holes over a 2×2 cm^2 area without obvious defects, with a diameter of about 200 nm and a period of 380 nm, has been successfully obtained. Figure 2(b) presents a cross-sectional profile of the surface along the white reference line drawn in Fig. 2(a). The Ni nanodisks were then electrodeposited in the patterned photoresist template that can be removed eventually. The height of the nanodisks is 125 nm. Figure 2(c) shows a typical top view of the sample observed by a scanning electron microscope; the diameters of the nanodisks have a relatively good uniformity ranging from 190 to 210 nm except for some defects. As we can see, all of the geometric parameters of the nanodisks including the period, diameter, and height can be controlled by the experimental process precisely and independently, which holds significant potential in the fabrication of macroscopic plasmonic devices.

III. RESULTS AND DISCUSSION

A. Tunable Fano resonance

The optical properties and the corresponding SP modes are strongly related to the polarization state of the incident light since it could be either s polarized or p polarized. In the rectangular coordinate system illustrated in Fig. 3(a), the electric field of s-polarized light is perpendicular to the incident plane and parallel to the xy plane. For this configuration, the free electrons in the nanodisks can oscillate collectively, driven by the electromagnetic wave. This oscillation is the origin of LSPs and can be properly described as a damped harmonic oscillator [6,8,17]. In contrast, the electric field of p-polarized light lies in the incident plane. It has an additional z-axis component besides the xy-plane component. On one hand, it is also possible for the LSP mode to be excited due to the presence of the xy-plane component, similar to the s-polarized situation. On the other hand, the z-axis component of the electric field can lead to a charge accumulation at the interface between the metal surface and air. This charge accumulation is essential

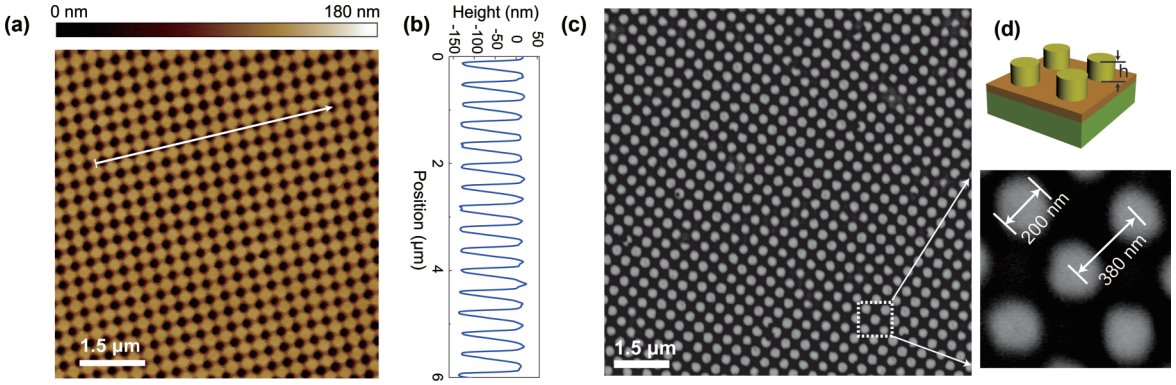

FIG. 2. Topography of the magnetoplasmonic structure. (a) Atomic force microscopy image of the photoresist pattern fabricated by interference lithography. (b) Cross-sectional profile of the surface along the white reference line drawn in Fig. 2(a). The height of the photoresist is 150 nm and the period is 380 nm. (c) Scanning electron micrograph of the magnetoplasmonic structure. A randomly selected area and its enlarged image are indicated by the white dotted box and arrows. The diameter of the nanodisks is approximately 200 nm. (d) Three-dimensional model of the magnetoplasmonic structure.

for the emergence of SPPs. In addition, the momentum match condition in a 2D periodic nanostructure is related to the relative orientation between the sample and the incoming light, viz., to both incident angle θ and azimuthal angle φ. The azimuthal angle φ is defined by the angle between the incident plane and the x axis along one of the basic directions of the square lattice. As depicted in Fig. 3(b), for the 380-nm-period array at $\varphi = 0^\circ$, the expected positions λ_0 exciting the $(-1,0)$ order SPP mode increases from 400 to 760 nm when θ changes from 0° to 90°. The simultaneously excited LSP and SPP modes render a possibility to obtain Fano resonance via the p-polarized light.

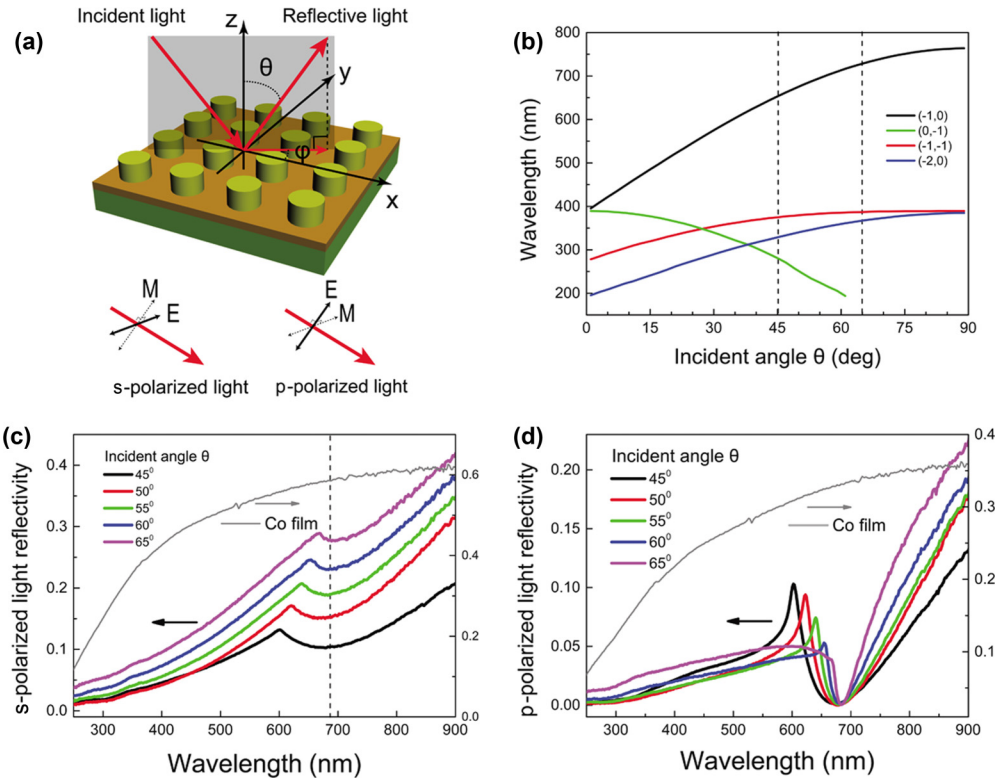

FIG. 3. Realization of Fano resonance. (a) A rectangular coordinate system is built on the sample; the x axis and y axis are along the basic directions of the square lattice. The relative orientation between the incident light and the sample is defined by the incident angle θ and azimuthal angle φ. Two configurations of polarization are explored: s polarized with the electric field perpendicular to the incident plane, and p polarized where the electric field lies in the incident plane. (b) The θ dependence of the calculated spectral positions to excite SPP modes for several diffraction orders ($\varphi = 0^\circ$). (c),(d) Measured reflectivity of the sample (left axis) at different θ and Co continuous film at $\theta = 45^\circ$ (right axis) versus wavelength for s-polarized light (c), and p-polarized light (d), maintaining $\varphi = 0^\circ$.

In Figs. 3(c) and 3(d), we show the reflectivity spectra of the sample at different θ ($\varphi = 0^\circ$), with a continuous Co film as reference. The spectrum for the continuous Co film at $\theta = 45^\circ$ is found to be monotonously increasing with the wavelength, while at each angle of incidence an obvious dip with a broad spectral range can be observed for the s-polarized light. This dip indicates the energy absorption related to the excitation of LSPs in the Ni nanodisks. In addition, the spectral location for the excitation of LSPs has a weak dependence upon the incident angle and shows an accurate corresponding relation to Fig. 1(a). But the total reflectivity is the combination of the Ni nanodisks and the bottom Co film. The reflectivity of the bottom layer gradually increases with θ and takes a major contribution. Thus it is reasonable that the minimum location is mainly fixed at about 680 nm, while the shape of the dip becomes narrower as θ increases from 45° to 65°. Interestingly, an obvious Fano-type asymmetric profile, which is a reflection maximum closely followed by a minimum, is observed in the reflective spectra for p-polarized light in Fig. 3(d). The Fano resonance appears in the spectrum range where the LSP and SPP modes are excited simultaneously, which reveals the strong coupling between them. The free electrons at the sample surface are involved in two different kinds of collective actions. So the constructive and destructive interferences between the narrow SPP mode and the broad LSP mode give rise to strong enhancement (reflection minima) and strong suppression (reflection maxima) of the absorption, respectively. The spectral position of the maximum in the Fano profile shows a redshift with θ increasing, similar to the trend of the excitation positions of SPPs. It confirms that because of utilizing the tunable SPP mode to couple with the LSP mode to form the Fano resonance, the Fano-like spectrum gets the tunability. On the other hand, due to the Fano resonance, the SPP mode in our sample shows a kind of localized character when its excitation wavelength matches the LSP position, which leads to the fact that the minimum of the Fano-like spectrum is almost stable at 680 nm. The strong coupling between the LSP and SPP modes is commonly indicated by an anticrossing behavior of the dispersion relations, as discussed in previous works [38–40]. Moreover, as θ increases, the xy-plane component of the electric field gradually decreases, but on the contrary, the z-axis component increases. The oscillation cannot happen in the z-axis direction (or at least not in the same spectral region) due to the direct contact between the nanodisks and the bottom Co film, so the LSP mode is weakening as θ increases. This leads to the dominance of the pure SPP mode at $\theta = 65^\circ$, and the Fano line shape degenerates to a simple dip.

In order to verify the corresponding SP modes, we numerically simulate the distribution of the electric field intensity $|\mathbf{E}|$ near the top surface of the nanodisks. The target plane is depicted in Fig. 4(a). For the s-polarized light in Fig. 4(b), a dipole oscillation mode along the y axis can be unambiguously demonstrated by the symmetric distribution of an enhanced electric field at $\lambda = 680$ nm, which corresponds to the minimum position in the reflective spectrum. Interestingly, for the p-polarized situation in Figs. 4(c)–4(f), we can clearly see the coexistence of the dipole and propagating modes. The dipole oscillation is along the x axis, orthogonal to the dipole mode excited by s-polarized light, while the wavelike field distribution in the gaps between the disks indicates a propagating charge-density wave induced by the SPPs excitation. Furthermore, the distribution pattern varies dramatically with only a small change in wavelength of the incident light, which corresponds to the steep drop stage of the Fano profile. This particular property may be valuable in applications such as sensors or optical switches. It also demonstrates that the SP excitation around the Fano resonance can be switched by tuning the frequency or phase differences between the LSP and SPP modes [41,42]. Especially at 650 nm in Fig. 4(e), the near field is dramatically enhanced and regularly confined within the square lattice, much stronger than the purely LSP mode in Fig. 4(b). As there is a transfer of characters between the localized and propagating modes when the LSP and SPP modes interact [43,44], the SPP mode has lost its original propagating character and become strongly localized. In order to show the confinement effects better, we simulate the phase of E_x for the p-polarized light at two typical wavelengths, $\lambda = 600$ nm and $\lambda = 650$ nm. In Fig. 4(g), we can clearly see the propagating mode, whereas in Fig. 4(h) there are obvious phase changes in the gaps between the disks. In Fig. 4(i), we particularly show the phase along the dotted line in Figs. 4(g) and 4(h). At $\lambda = 600$ nm, the areas from −290 nm to −90 nm and 90 nm to 290 nm, corresponding to the positions of the disks, show the consistent phase, rather than changing with the wave-front phase (the dotted line). It is explained as the collective motion of the electrons on the surface of the disks. This is more evident when $\lambda = 650$ nm, which is closer to the peak of the LSP mode. For the area between two adjacent disks from −90 nm to 90 nm, the increase tendency of the phase of the SPP mode is in coincidence with the change of the wave-front phase at $\lambda = 600$ nm. When $\lambda = 650$ nm, the phase of SPP mode reveals a much more violent change compared with the wave-front phase. The interaction between the LSP and SPP localizes the phase change, which should be finished during a period from −90 nm to 290 nm when $\lambda = 600$ nm, in the gap between two disks. Consequently, the free electrons from all over the sample surface, including the exposed part of the Co film, behave as localized oscillators that give rise to the astonishing distribution pattern.

Furthermore, the Fano resonance can also be tuned by changing the azimuthal angle, due to the in-plane anisotropy induced by two sets of reciprocal lattice vectors in the xy plane. The 2D square array has a fourfold rotational symmetry, hence the optical response will exhibit a similar feature. As shown in Fig. 5(a), the reflection spectra are symmetric at about $\varphi = 45^\circ$. The peak of the Fano line shape shows a blueshift when φ increases from 0° to 45°, but a redshift from 45° to 90°. It can be explained by the calculated φ dependence of spectral positions of SPPs in Fig. 5(b). When φ changes from 0° to 90°, three diffraction orders of SPPs play a part in the optical region. The λ_0 of the (−1,0) mode decreases from 650 nm at $\varphi = 0^\circ$, while that of the (0,−1) mode increases at the same time, and they eventually cross over at 520 nm ($\varphi = 45^\circ$). The (−1,−1) mode presents a relatively weak dependence on φ, and it ranges from 375 to 460 nm. These results confirm the excellent periodicity of the Ni array in our sample. Naturally, it should be expected that the MO response will exhibit a similar dependence on the relative orientation of the incoming light.

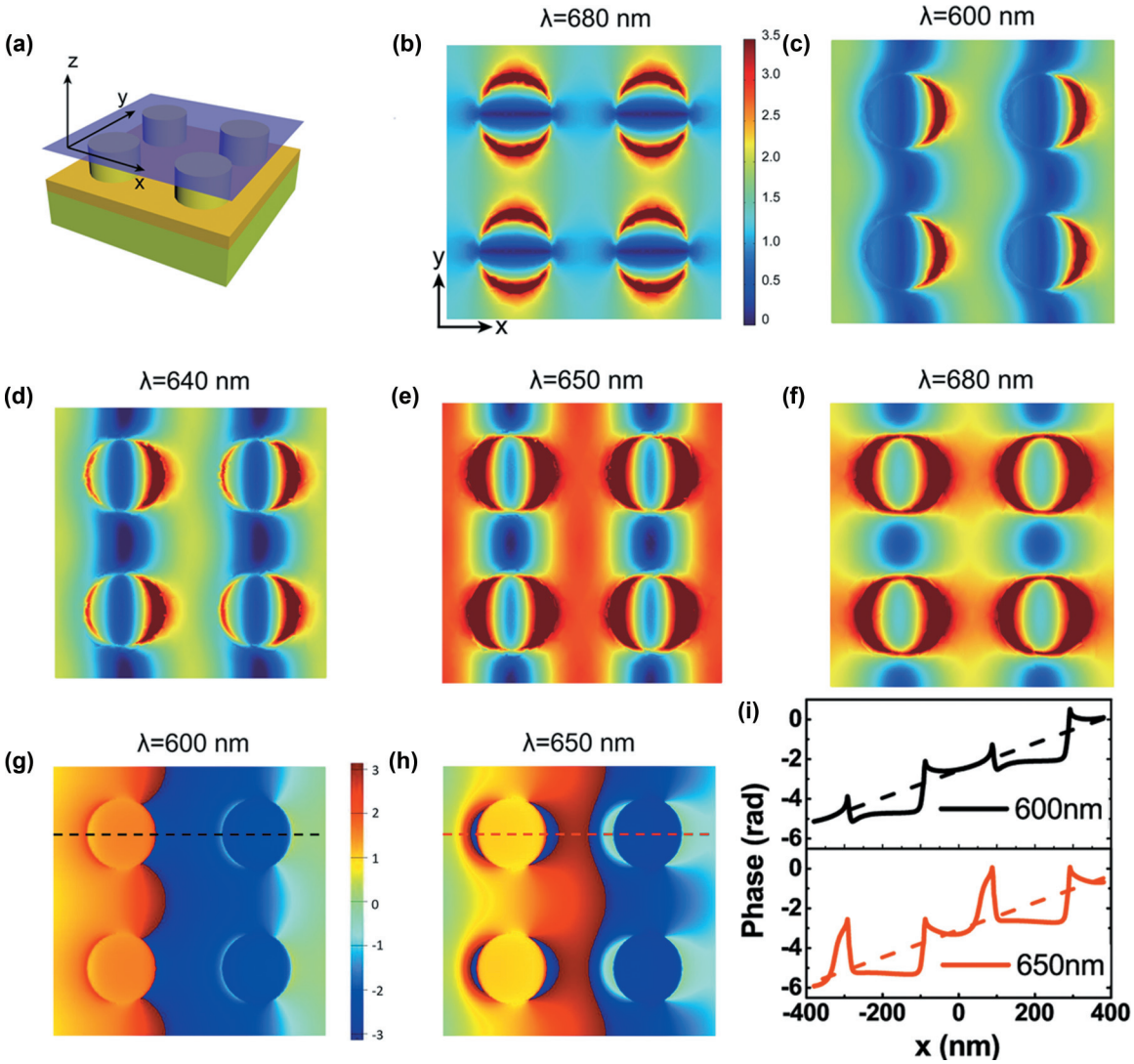

FIG. 4. Distribution of electric field intensity. (a) Target plane (blue-color plane) for the numerical simulations. (b) Field distribution pattern for s-polarized light at 680 nm ($\theta = 45^\circ$, $\varphi = 0^\circ$), corresponding to the reflectivity minimum position. (c)–(f) Field distribution pattern for p-polarized light at several wavelengths in the region of Fano resonance ($\theta = 45^\circ$, $\varphi = 0^\circ$). (g),(h) The phases of E_x for the p-polarized light at $\lambda = 600$ nm and $\lambda = 650$ nm. (i) The phase along the dotted line in (g) and (h).

B. Fano-resonance-mediated Kerr rotation reversal

The MO Kerr rotation is based on the small rotation of the polarization plane of the reflective light when a magnetic field is applied to a FM metal. It originates from the nondiagonal element of the dielectric tensor related to the spin-orbit coupling, and it is an intrinsic property of the material that cannot be controlled freely. In magnetoplasmonic systems, the influence of the SP modes on the MO activity is mainly attributed to two effects: one is associated with the decrease of reflectivity of the system due to the SP excitations, which is of purely optical origin, and the other is the concentration of the electromagnetic field inside the MO active material and hence changes the MO response [4]. For the situation of SPPs, the optical part dominates as it usually gives rise to a reflectivity reduction, which simply produces an enhancement of the Kerr rotation. This effect has been demonstrated in either noble-metal/FM-metal multilayers [22,23] or perforated FM membranes [26–29], while for LSPs, the influence of the MO part is more important. It has been shown that the sign of the Kerr rotation of randomly separated Ni nanodisks on the glass substrate is reversed in the vicinity of the LSP resonance, which is absent in the optical region for Ni bulk or film [6,17]. Moreover, if we look into the literature carefully, there will be more evidence that the LSP in nanostructured FM metal is always accompanied by the sign change of Kerr rotation [18,19,45–47]. The Kerr rotation reversal is very likely a fundamental feature of the LSPs effect on the MO response in nanoconfined magnetoplasmonic systems.

An interesting question is what the MO Kerr rotation will be in a complex plasmonic system where the LSPs and SPPs coexist and are coherently coupled, such as the case of our samples, in which the overall MO response is caused by the combination of Ni nanodisks and Co film substrate. In the absence of LSPs and SPPs, the MO response is determined by the intrinsic properties of the materials. If just the SPPs are excited, the Kerr rotation will be simply enhanced due to

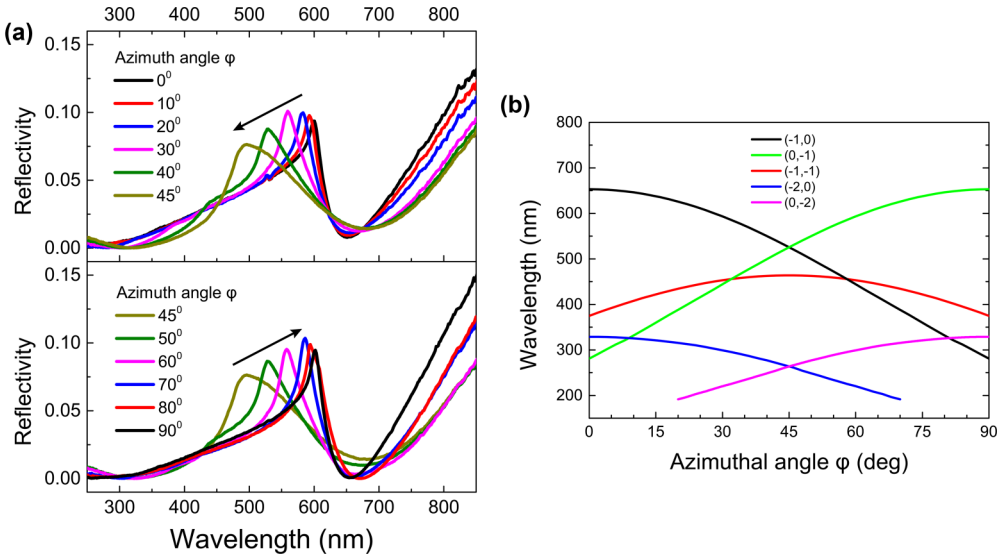

FIG. 5. Tunability of the Fano resonance. (a) Measured reflectivity of the sample at different φ from 0° to 45° and 45° to 90° versus wavelength for p-polarized light, maintaining $\theta = 45°$. (b) The φ dependence of the calculated spectral positions of SPPs for several diffraction orders ($\theta = 45°$).

the reduction of reflectivity. On the contrary, if just the LSPs are excited, the Kerr rotation induced by the Ni nanodisks may be reversed near the resonance but the Co substrate will not be affected. The overall Kerr signal is the sum of that induced by the Ni nanodisks and Co substrate. However, to modify the Kerr rotation of the whole system, the collective actions of the electrons in both LSPs and SPPs have to be effectively coupled. Therefore, there is a possibility to control the Kerr rotation of the whole sample by the Fano resonance, where LSPs and SPPs strongly interact. Figure 6(a) shows the longitudinal Kerr rotation spectrum at $\theta = 45°$. For the longitudinal configuration, the magnetization lies along the plane of incidence and parallel to the sample surface. Pure Co or Ni film exhibits a monotonous Kerr spectrum which maintains a positive value between 440 and 710 nm. However, for our sample, the sign of Kerr rotation is reversed at about 680 nm when $\varphi = 0°$ and at 540 nm when $\varphi = 45°$, respectively. Obviously, the reversal appears at the spectral positions in the region of Fano resonance and shows a similar blueshift behavior as φ increases. The simulation results in this figure (denoted by the blue and red arrows) can give us more insight into the electric field distribution at the reversal positions. In addition, the MO loops (the Kerr rotation versus the magnetic field) were measured at some specific wavelengths as shown in Figs. 6(b)–6(e). In Fig. 6(d), we show the MO loops at the wavelength near the reversed position of the Kerr rotation. The direction of the loop is opposite to each other, corresponding to the sign reversal. The line shape of the loop does not show great abnormality. Therefore, we consider the Kerr rotation reversal as the collective action of both Co and Ni, due to the localization effect of the SPP mode, which is considered as the effect of the Fano resonance in our sample. The same results are shown in Fig. 6(e) when $\varphi = 45°$. The maximal Kerr rotation is $-0.09°$ at 710 nm, while it is 0.06° and 0.02° for Co and Ni continuous film at the same wavelength. The comparison would be more remarkable if we take into account the volume fraction, that is, 78.3% for Co and 21.7% for Ni. These results confirm that the Fano

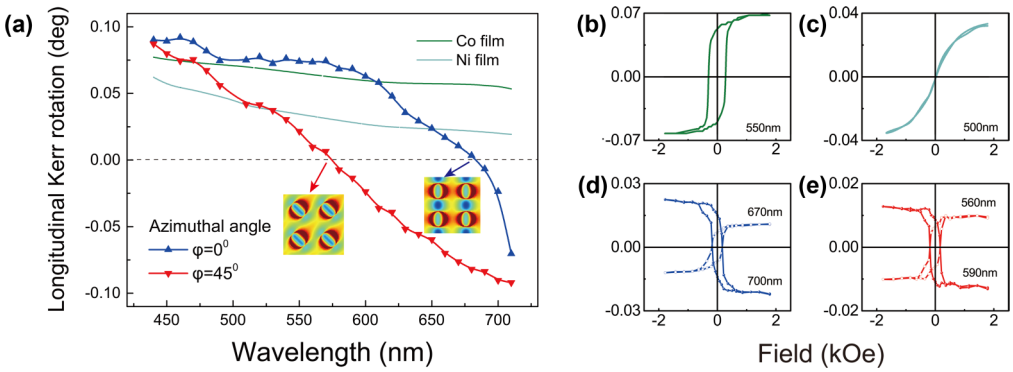

FIG. 6. Longitudinal MO Kerr rotation for p-polarized light. (a) Measured Kerr rotation angle versus wavelength for the Co film, Ni film, and the magnetoplasmonic structure at $\varphi = 0°$ and $\varphi = 45°$ ($\theta = 45°$). Insets are the simulation results of the field distribution pattern at two Kerr rotation reversal positions, indicated by the blue and red arrows. (b)–(e) MO loops at several wavelengths for the Co film (b), Ni film (c), and the magnetoplasmonic structure at $\varphi = 0°$ (d) and $\varphi = 45°$ (e).

resonance leads to both enhancement and reversal of the Kerr signal.

It is very complicated to accurately calculate the effect of Fano resonance on the MO response, because one has to take full consideration of the interplay between fundamental electronic structure, optical and magnetic response of the system. However, the underlying physics can be properly captured by a simplified model. As we know, in the visible range, the major part that contributes to the light-matter interaction is the strong interaction between the electric field and the huge amounts of free electrons in the metal (neglect the interband transition). The Kerr rotation can be understood by considering that the external magnetic field applies a transverse Lorentz force on the action of the electrons, and consequently changes the polarization of the reflected light. In our sample, not only the LSP mode but also the SPP mode can be switched to a strongly localized mode due to the coupling between the LSP and SPP modes as demonstrated above. We may reasonably assume that the action of free electrons in this localized resonant mode, which is analogous to the simple LSP mode excited in an individual (or well separated) nanostructure, can be described by a dipole oscillator with an intrinsic resonance frequency ω_0 driven by the light wave [8,48]. Then the phase delay of the oscillation relative to the driving force is given by

$$\delta = \tan^{-1}\left(\frac{\omega\gamma}{\omega_0^2 - \omega^2}\right), \tag{1}$$

where γ is the damping parameter and ω is the driving frequency. Obviously, δ crosses over $\frac{\pi}{2}$ in the vicinity of the singularity $\omega = \omega_0$. (If $\omega < \omega_0$, $0 < \delta < \frac{\pi}{2}$; and if $\omega > \omega_0$, $\frac{\pi}{2} < \delta < \pi$.) Namely, the free electrons oscillate in phase with the driving wave for $\omega < \omega_0$, but out of phase for $\omega > \omega_0$, so the direction of the Lorentz force and eventually the MO response change sign near the resonance. Notice that for the situation of the solely SPP mode, the free electrons do not behave as dipole oscillators since they experience no restoring forces when they are displaced (or suppose $\omega_0 = 0$), therefore neither obvious change of δ nor reversal of Kerr rotation can be observed. As a case in point, Ctistis *et al.* [26] confirmed that the enhancement of the MO response in periodically perforated Co films is directly connected to the SPP excitation. Surprisingly, the results of the larger-holes samples show a change in sign of the Kerr rotation, which are very different from the situation in the small-holes samples. Apparently, this can be explained by the localization of SPP modes when the diameter of the holes is considerably large.

IV. EXPERIMENTAL DETAILS

Sample fabrications. The magnetoplasmonic structures were fabricated as follows. First, a 50-nm-thick Co film was deposited on Si (100) substrate at room temperature by dc magnetron sputtering .The base pressure is 2×10^{-5} Pa and the Ar gas pressure is 0.5 Pa. A 150-nm-thick positive photoresist (Allresist, AR-P 3170) was spin-coated on the Co layer at 5000 rpm followed by a prebake at 95 °C for 1 min. Then the photoresist was patterned by a homemade Lloyd's-mirror interference lithography system with a commercial 325/442 nm wavelength He-Cd laser. For large-area lithography, the diameter of the laser beam was preexpanded to 8.0 cm. The period of the fringe pattern can be given by $\lambda/2 \sin\theta$, where λ is the laser wavelength and θ is the half angle of intersection of the laser beams. The sample was exposed twice separated by an in-plane rotation of 90° and immersed in a developing solution for 45 s (Allresist, AR 300–26 diluted 1:5 with deionized water). A square lattice pattern of holes with controllable diameter can be produced by properly adjusting the exposure dose. The residual resist inside the holes was removed using O_2 plasma etching for 15 s. In the next step, nickel nanodisks were electrodeposited into the template from a solution containing 15 g/L $NiSO_4 \cdot 6H_2O$ and 30 g/L H_3BO_3. The deposition current density was set to 0.1 mA/cm^2. After deposition, the photoresist was eventually removed by dipping samples into acetone in a 60 °C water bath for about 10 min.

Optical reflectivity and magneto-optical Kerr rotation measurements. The optical reflectivity was measured by spectroscopic ellipsometry with a white light source at different incident angles from 45° to 65°. The light was focused on the sample into a spot with a diameter of ∼0.5 mm. To perform measurements at different azimuthal angles, the sample was mounted on an in-plane rotational stage. The reflectivity spectra were obtained by the ratio of the zero-order reflective signal of the samples to a base line of the light source. For MO measurements we used a homemade MO Kerr system consisting of a pulsed laser with 20 Hz repetition rate working in the wavelength range of 410–800 nm. The light spot diameter is approximately 1 mm. Magnetic fields up to 2.5 kOe were applied in longitudinal configuration using an electromagnet. The overall angle resolution of the system was below 0.001°.

V. SUMMARY

In conclusion, based on the interference lithography and electrochemical deposition, we have fabricated large-area periodic plasmonic systems by exclusive FM metals with adjustable geometric parameters. This so-called magnetoplasmonic structure shows an extraordinary Fano resonance, that is, the effective coupling between the SPP mode related to the periodicity and the LSP mode trapped on the nanodisks. Besides the conventional enhancement effect, we also demonstrated the Kerr rotation reversal related to the strongly localized effect of the SPP mode due to the Fano resonance. The concerted actions of free electrons in magnetoplasmonic materials can affect the MO properties in a very extensive way, not only changing the magnitude of Kerr rotation but also modifying the phase. We provide a flexible and excellent routine to design coupled plasmonic devices in macroscopic scale. We also expect manipulation of a more pronounced MO response by incorporating our method with more efficient MO materials. For example, the HfO_2/Co/HfO_2/Al/substrate composite structure can exhibit a surprisingly giant polar Kerr rotation of 7.92° [49]. Realization of a controllable sign change of the Kerr rotation gives rise to the new concept of polarization-resolved MO light modulation and MO-based biochemical sensors, which might represent ultrahigh sensitivity to the refractive index and an unlimited value of figure of merit, alternative to the presently developed plasmon-based ones [6]. Furthermore, the Fano resonance promises

fascinating prospects in discovering novel plasmon-boosted phenomena, not merely the MO effects. Some have been proposed or demonstrated recently, but many not yet. We hope our work can put forward developments toward the realization of Fano resonance and the outstanding controllability of MO responses in magnetoplasmonic nanostructures.

ACKNOWLEDGMENTS

This work is supported by the National Key project of Fundamental Research of China (Grant No. 2012CB932304) and the Natural Science Foundation of China (Grants No. 11374146 and No. U1232210).

[1] G. Armelles, A. Cebollada, A. García-Martín, J. M. García-Martín, M. U. González, J. B. González-Díaz, E. Ferreiro-Vila, and J. F. Torrado, J. Opt. A **11**, 114023 (2009).
[2] S. H. Fan, Nat. Photonics **4**, 76 (2010).
[3] V. V. Temnov, G. Armelles, U. Woggon, D. Guzatov, A. Cebollada, A. García-Martín, J. M. García-Martín, T. Thomay, A. Leitenstorfer, and R. Bratschitsch, Nat. Photonics **4**, 107 (2010).
[4] G. Armelles, A. Cebollada, A. García-Martín, and M. U. González, Adv. Opt. Mater. **1**, 10 (2013).
[5] M. Liu and X. Zhang, Nat Photonics **7**, 429 (2013).
[6] V. Bonanni, S. Bonetti, T. Pakizeh, Z. Pirzadeh, J. Chen, J. Nogués, P. Vavassori, R. Hillenbrand, J. Åkerman, and A. Dmitriev, Nano Lett. **11**, 5333 (2011).
[7] N. Maccaferri, K. E. Gregorczyk, T. V. de Oliveira, M. Kataja, S. van Dijken, Z. Pirzadeh, A. Dmitriev, J. Åkerman, M. Knez, and P. Vavassori, Nat. Commun. **6**, 6150 (2015).
[8] J. Chen, P. Albella, Z. Pirzadeh, P. Alonso-González, F. Huth, S. Bonetti, V. Bonanni, J. Åkerman, J. Nogués, P. Vavassori, A. Dmitriev, J. Aizpurua, and R. Hillenbrand, Small **7**, 2341 (2011).
[9] V. I. Belotelov, I. A. Akimov, M. Pohl, V. A. Kotov, S. Kasture, A. S. Vengurlekar, A. V. Gopal, D. R. Yakovlev, A. K. Zvezdin, and M. Bayer, Nat. Nanotechnol. **6**, 370 (2011).
[10] J. Y. Chin, T. Steinle, T. Wehlus, D. Dregely, T. Weiss, V. I. Belotelov, B. Stritzker, and H. Giessen, Nat. Commun. **4**, 1599 (2013).
[11] V. I. Belotelov, L. E. Kreilkamp, I. A. Akimov, A. N. Kalish, D. A. Bykov, S. Kasture, V. J. Yallapragada, A. V. Gopal, A. M. Grishin, S. I. Khartsev, M. Nur-E-Alam, M. Vasiliev, L. L. Doskolovich, D. R. Yakovlev, K. Alameh, A. K. Zvezdin, and M. Bayer, Nat. Commun. **4**, 2128 (2013).
[12] I. Zubritskaya, K. Lodewijks, N. Maccaferri, A. Mekonnen, R. K. Dumas, J. Åkerman, P. Vavassori, and A. Dmitriev, Nano Lett. **15**, 3204 (2015).
[13] K. Lodewijks, N. Maccaferri, T. Pakizeh, R. K. Dumas, I. Zubritskaya, J. Åkerman, P. Vavassori, and A. Dmitriev, Nano Lett. **14**, 7207 (2014).
[14] B. Luk'yanchuk, N. I. Zheludev, S. A. Maier, N. J. Halas, P. Nordlander, H. Giessen, and C. T. Chong, Nat. Mater. **9**, 707 (2010).
[15] C. Wu, A. B. Khanikaev, R. Adato, N. Arju, A. A. Yanik, H. Altug, and G. Shvets, Nat. Mater. **11**, 69 (2012).
[16] A. E. Miroshnichenko, S. Flach, and Y. S. Kivshar, Rev. Mod. Phys. **82**, 2257 (2010).
[17] N. Maccaferri, A. Berger, S. Bonetti, V. Bonanni, M. Kataja, Q. H. Qin, S. van Dijken, Z. Pirzadeh, A. Dmitriev, J. Nogués, J. Åkerman, and P. Vavassori, Phys. Rev. Lett. **111**, 167401 (2013).
[18] J. B. González-Díaz, A. García-Martín, J. M. García-Martín, A. Cebollada, G. Armelles, B. Sepúlveda, Y. Alaverdyan, and M. Käll, Small **4**, 202 (2008).
[19] J. B. González-Díaz, A. García-Martín, G. Armelles, D. Navas, M. Vázquez, K. Nielsch, R. B. Wehrspohn, and U. Gösele, Adv. Mater. **19**, 2643 (2007).
[20] J. C. Banthí, D. Meneses-Rodríguez, F. García, M. U. González, A. García-Martín, A. Cebollada, and G. Armelles, Adv. Mater. **24**, OP36 (2012).
[21] V. L. Krutyanskiy, I. A. Kolmychek, E. A. Gan'shina, T. V. Murzina, P. Evans, R. Pollard, A. A. Stashkevich, G. A. Wurtz, and A. V. Zayats, Phys. Rev. B **87**, 035116 (2013).
[22] J. B. González-Díaz, A. García-Martín, G. Armelles, J. M. García-Martín, C. Clavero, A. Cebollada, R. A. Lukaszew, J. R. Skuza, D. P. Kumah, and R. Clarke, Phys. Rev. B **76**, 153402 (2007).
[23] E. Ferreiro-Vila, J. B. González-Díaz, R. Fermento, M. U. González, A. García-Martín, J. M. García-Martín, A. Cebollada, G. Armelles, D. Meneses-Rodríguez, and E. M. Sandoval, Phys. Rev. B **80**, 125132 (2009).
[24] J. B. González-Díaz, J. M. García-Martín, A. García-Martín, D. Navas, A. Asenjo, M. Vázquez, M. Hernández-Vélez, and G. Armelles, Appl. Phys. Lett. **94**, 263101 (2009).
[25] M. V. Sapozhnikov, S. A. Gusev, V. V. Rogov, O. L. Ermolaeva, B. B. Troitskii, L. V. Khokhlova, and D. A. Smirnov, Appl. Phys. Lett. **96**, 122507 (2010).
[26] G. Ctistis, E. Papaioannou, P. Patoka, J. Gutek, P. Fumagalli, and M. Giersig, Nano Lett. **9**, 1 (2009).
[27] E. T. Papaioannou, V. Kapaklis, P. Patoka, M. Giersig, P. Fumagalli, A. García-Martín, E. Ferreiro-Vila, and G. Ctistis, Phys. Rev. B **81**, 054424 (2010).
[28] J. F. Torrado, E. T. Papaioannou, G. Ctistis, P. Patoka, M. Giersig, G. Armelles, and A. García-Martín, Phys. Status Solidi RRL **4**, 271 (2010).
[29] E. T. Papaioannou, V. Kapaklis, E. Melander, B. Hjörvarsson, S. D. Pappas, P. Patoka, M. Giersig, P. Fumagalli, A. García-Martín, and G. Ctistis, Opt. Express **19**, 23867 (2011).
[30] G. Armelles, A. Cebollada, A. García-Martín, M. U. González, F. García, D. Meneses-Rodríguez, N. de Sousa, and L. S. Froufe-Pérez, Opt. Express **21**, 27356 (2013).
[31] M. Kataja, T. K. Hakala, A. Julku, M. J. Huttunen, S. van Dijken, and P. Törmä, Nat. Commun. **6**, 7072 (2015).
[32] A. Lovera, B. Gallinet, P. Nordlander, and O. J. Martin, ACS Nano **7**, 4527 (2013).
[33] N. Verellen, Y. Sonnefraud, H. Sobhani, F. Hao, V. V. Moshchalkov, P. Van Dorpe, P. Nordlander, and S. A. Maier, Nano Lett. **9**, 1663 (2009).
[34] N. Maccaferri, J. B. González-Díaz, S. Bonetti, A. Berger, M. Kataja, S. van Dijken, J. Nogués, V. Bonanni, Z. Pirzadeh,

A. Dmitriev, J. Åkerman, and P. Vavassori, Opt. Express **21**, 9875 (2013).
[35] S. A. Maier, *Surface Plasmonics: Fundamentals and Application* (Springer, New York, 2007), p. 44.
[36] C. A. Ross, H. I. Smith, T. Savas, M. Schattenburg, M. Farhoud, M. Hwang, M. Walsh, M. C. Abraham, and R. J. Ram, J. Vac. Sci. Technol. B **17**, 3168 (1999).
[37] D. Xia, Z. Ku, S. C. Lee, and S. R. J. Brueck, Adv. Mater. **23**, 147 (2011).
[38] Y. Chu and K. B. Crozier, Opt. Lett. **34**, 244 (2009).
[39] A. Ghoshal, I. Divliansky, and P. G. Kik, Appl. Phys. Lett. **94**, 171108 (2009).
[40] A. Christ, T. Zentgraf, S. G. Tikhodeev, N. A. Gippius, J. Kuhl, and H. Giessen, Phys. Rev. B **74**, 155435 (2006).
[41] H. Liu, G. X. Li, K. F. Li, S. M. Chen, S. N. Zhu, C. T. Chan, and K. W. Cheah, Phys. Rev. B **84**, 235437 (2011).
[42] Y. J. Bao, R. W. Peng, D. J. Shu, M. Wang, X. Lu, J. Shao, W. Lu, and N. B. Ming, Phys. Rev. Lett. **101**, 087401 (2008).
[43] J. Cesario, R. Quidant, G. Badenes, and S. Enoch, Opt. Lett. **30**, 3404 (2005).
[44] J. F. Torrado, J. B. González-Díaz, M. U. González, A. García-Martín, and G. Armelles, Opt. Express **18**, 15635 (2010).
[45] J. B. González-Díaz, B. Sepúlveda, A. García-Martín, and G. Armelles, Appl. Phys. Lett. **97**, 043114 (2010).
[46] D. Meneses-Rodríguez, E. Ferreiro-Vila, P. Prieto, J. Anguita, M. U. González, J. M. García-Martín, A. Cebollada, A. García-Martín, and G. Armelles, Small **7**, 3317 (2011).
[47] S. Zhang, S. Tang, J. Gao, X. Luo, W. Xia, and Y. Du, Solid State Commun. **170**, 19 (2013).
[48] J. Zuloaga and P. Nordlander, Nano Lett. **11**, 1280 (2011).
[49] S. Zhang, J. Gao, W. Xia, X. Luo, S. Tang, and Y. Du, J. Appl. Phys. **114**, 064308 (2013).